Nanoscale Advances

ROYAL SOCIETY OF CHEMISTRY

COMMUNICATION

View Article Online
View Journal | View Issue

Cite this: *Nanoscale Adv.*, 2025, **7**, 4018

Received 14th March 2025
Accepted 16th May 2025

DOI: 10.1039/d5na00243e

rsc.li/nanoscale-advances

Plasmonic behaviour of poly(2-ethyl-2-oxazoline)-coated gold nanoparticles for sensing and temperature-control applications†

Oleg Yeshchenko, *[a] Léa Daoud, [b] Pavlo Khort,[a] Oles Fedotov,[a] Julien-Bilal Zinoune,[c] Georges Boudebs, [c] Tony Breton, [d] Catherine Passirani, [b] Patrick Saulnier[b] and Oksana Krupka *[ab]

Gold nanoparticles functionalized with xanthate-poly(2-ethyl-2-oxazoline) (PEtOx-AuNPs) were investigated as thermoresponsive hybrid nanomaterials with tunable optical and thermal properties. The PEtOx-AuNPs exhibited changes in surface plasmon resonance (SPR) and amplified Surface-Enhanced Raman Scattering (SERS) signals during the reversible lower critical solution temperature (LCST) transition of the PEtOx ligand. The effect of the PEtOx coating on the photophysical properties of AuNPs, particularly on heat generation efficiency upon photoexcitation by Z-scan photothermal lens spectroscopy, was investigated. The results demonstrate the potential of PEtOx-AuNPs for applications in temperature-sensitive drug delivery, photothermal therapy, nanoscale heat generation, and photonic devices.

Gold nanoparticles (AuNPs) have attracted great attention of researchers across diverse fields since their first formulation in 1857 by M. Faraday.[1] This early experiment with colloidal gold initiated the development of nanoscience and nanotechnology. AuNPs possess a range of unique properties that make them highly valuable in scientific and technological fields. Notably, AuNPs exhibit particularly strong absorption and scattering of light within specific spectral bands, a phenomenon attributed to surface plasmon resonance (SPR) excitation.[2,3] In particular, SPR enhances the value of AuNPs for biomedical applications including biosensing, imaging, and photothermal or photodynamic therapy.[4–6] The optical properties of AuNPs can be tuned by their size and shape.[7] AuNPs are generally non-toxic and more compatible with cell environments than other types of nanomaterials used in *in vitro* and *in vivo* applications, making them suitable for use in medical applications such as drug delivery[8] and imaging[9] and as therapeutic agents.[10] The surface of AuNPs can be functionalized with various ligands or biomolecules for targeted drug delivery or specific biomolecular detection.[11] With advancements in characterization and manufacturing and the increasing demand for universal, multi-profile nanomaterials, the decoration of nanoparticles presents new challenges and opportunities. All these diverse and exceptional properties make AuNPs a versatile and powerful tool, from materials science to medicine.

Nanobiology and nanomedicine are driving the development of new hybrid functional materials based on biocompatible,[12,13] thermoresponsive polymers, which serve as the foundation for creating temperature-controlled nanoactuators.[14] Among these polymers, those exhibiting a Lower Critical Solution Temperature (LCST) phase transition hold particular significance.

During the LCST transition, polymers undergo a shift from a hydrophilic to a hydrophobic state, resulting in rapid and pronounced shrinkage.[15] This transformation is reversible and highly sensitive to temperature changes, making these polymers exceptionally important for applications that require controlled, temperature-responsive properties. One of the most versatile and well-tunable thermoresponsive polymers is poly-oxazoline (POx),[16,17] which has gained considerable attention due to its unique combination of thermosensitive properties,[18] excellent biocompatibility,[19] and lack of immune response.[20] POx enhances circulation time *in vivo* and is emerging as a superior alternative among synthetic polymers recently investigated.[21] POx exhibits excellent solubility in both hydrophilic and hydrophobic solvents and a hydrophilic–lipophilic balance easily tunable through synthesis by changing the nature of the acyl group.[22] Core–shell nanoparticles with a metal core (such as Au) and a thermoresponsive polymer shell effectively combine the sensing capabilities of the plasmonic metal shell with the actuator properties of the polymer shell at the nanoscale. During the LCST transition, water molecules are expelled from the space between neighbouring polymer chains,

[a]*Taras Shevchenko National University of Kyiv, 60 Volodymyrska str., 01033 Kyiv, Ukraine*

[b]*Univ Angers, Inserm, CNRS, MINT, SFR ICAT, F-49000 Angers, France*

[c]*Univ Angers, LPHIA, SFR MATRIX, 2 Bd Lavoisier, F-49000 Angers, France*

[d]*Univ Angers, CNRS, MOLTECH-Anjou, SFR MATRIX, F-49000 Angers, France*

† Electronic supplementary information (ESI) available: Synthetic details and characterization, X-ray photoelectron spectra, extinction spectra, LCST transition, Raman spectra, and Z-scan photothermal lens spectra. See DOI: https://doi.org/10.1039/d5na00243e

causing the polymer chains to contract. Consequently, the polymer shell surrounding the AuNPs becomes thinner and denser. Additionally, the hydrophobicity of the polymer shell above the LCST transition point is expected to induce AuNP aggregation. Together, these effects are expected to have a significant impact on SPR and Raman scattering of the polymer enhanced by the plasmonic field.

In this study, we investigated the plasmonic optical heating and thermoresponsive optical switching phenomena of α-methyl-ω-ethylxanthato-poly(2-ethyl-2-oxazoline) decorated AuNPs (PEtOx-AuNPs) using newly developed Z-scan photothermal lens spectroscopy (Zscan-TLS),[23] dynamic light scattering (DLS), light extinction and Surface-Enhanced Raman Scattering (SERS) methods. Investigation of the heating capacity of polymer coated AuNPs is a crucial step in developing efficient platforms for both distributed and localized heat generation. Among these, polyoxazoline-coated AuNPs stand out due to their unique thermoresponsive properties, offering broad potential for applications ranging from photonic devices to temperature-sensitive drug delivery systems.

Results and discussion

Ligand exchange is a versatile technique that can enhance the stability, functionality, and biocompatibility of AuNPs, broadening their potential applications across fields such as biomedicine, environmental science, and nanotechnology.[24,25]

α-methyl-ω-ethylxanthato-poly(2-ethyl-2-oxazoline) (PEtOx) with a degree of polymerization (DP) of 39, number-average molecular weight (M_n) of 3.9 kg mol^{-1} and dispersity ($Đ$) of 1.25 was synthesized *via* cationic ring-opening polymerization using methyl *p*-toluenesulfonate as the initiator. The polymerization was terminated using potassium ethyl xanthogenate yielding the corresponding end-functionalized polymer.[26] The polymer characteristics were determined through size exclusion chromatography (SEC), in agreement with MALDI-TOF mass spectrometry and ^{1}HNMR spectra (synthetic details and characterization in Fig. S1 and S2 and Table S1, in the (ESI†).

Citrate buffer stabilized AuNPs, with a diameter of 40 nm and an optical density of approximately unity, were used for ligand exchange. This process involved replacing the citrate ions on the AuNP surface with xanthate-containing PEtOx ligands to introduce new functional properties (Fig. 1). Free xanthate- PEtOx ligands were removed from the PEtOx-AuNP colloid through three cycles of centrifugation and redispersion in Milli-Q ultrapure water. Partial ligand exchange resulted in double stabilization of the AuNP colloid by electrostatic repulsion and steric stabilization, preventing aggregation.[27] The xanthate capping ligand was selected for this study due to its superior stability against oxidation when compared to thiol analogues or carboxylic acid-containing ligands. Moreover, the formulation with the xanthate capping ligand exhibits significant thermal and pH stability.[28–31]

The formation of a PEtOx polymer coating around AuNPs was confirmed through a combination of transmission electron microscopy (TEM), X-ray photoelectron spectroscopy (XPS), DLS, light extinction spectroscopy and Raman scattering.

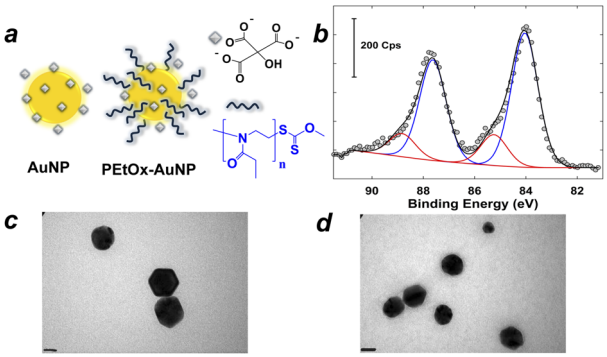

Fig. 1 (a) Schematic presentation of AuNPs before and PEtOx-AuNPs after ligand exchange; (b) Au4f core level spectra of PEtOx-AuNPs; (c) TEM image of citrate stabilized AuNPs (scale bar 18 nm); (d) TEM image of PEtOx-AuNPs (scale bar 20 nm).

These complementary techniques provided comprehensive characterization of the polymer shell, while the SPR was used as a sensor to detect and quantify the temperature-induced LCST phase transition of the polymer.

XPS measurements were performed on PEtOx-AuNPs after ligand exchange (see Fig. S4 for the survey spectrum, ESI†). In the Au4f core level spectra presented in Fig. 1d, the two main components at 84 and 87.6 eV are attributed to the Au^0 state.[32] The fitting-deconvolution procedure for the Au4f region revealed an additional pair of components at 85.2 and 88.8 eV that can be attributed to a Au$^{\delta+}$ state, typically observed in the presence of adsorbed thiolated species.[33] The adsorption of xanthate moieties is likely responsible for this oxidized state of the gold. This hypothesis is corroborated by the analysis of the S2p core level spectrum (Fig. S4, ESI†), where the binding energy of the two components (*i.e.* 163.2 and 164.3 eV) is typical of physisorbed sulfur atoms[33]

The temperature-dependent behaviour of the hydrodynamic diameter of PEtOx-AuNPs was thoroughly investigated using the DLS method. The results clearly confirm the presence of

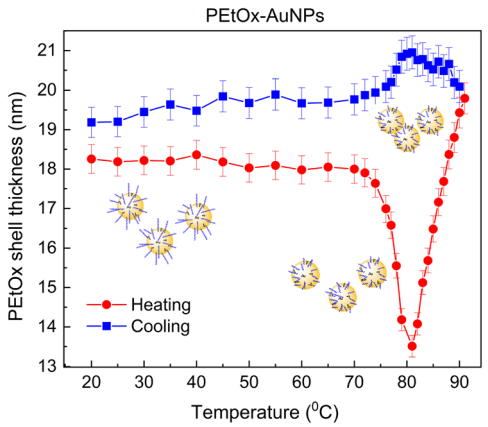

Fig. 2 Temperature dependence of DLS derived PEtOx shell thickness of PEtOx-AuNPs during the heating–cooling cycle in the temperature range 20–91–20 °C.

a polymer shell surrounding AuNPs. Fig. 2 illustrates the variation in shell thickness as a function of temperature, highlighting the LCST transition of the polymer.

The thickness of the PEtOx shell (d_s) was determined using $d_s = (d - d_c)/2$, where d is the hydrodynamic diameter of PEtOx-AuNPs and d_c = 40 nm is AuNP's core diameter. The results indicated that the shell thickness remained constant at 18 nm during heating in the range 20–60 °C.

As the temperature increases to 74 °C, the shell thickness sharply decreases to 13.5 nm, indicating polymer shrinkage during the LCST transition. Notably, the nanoparticles remain well-dispersed without aggregation up to this temperature. Further heating from 74 °C to 91 °C leads to a pronounced increase in shell thickness to 20 nm, suggesting NP aggregation. Upon reverse cooling from 91 °C to 82 °C, the final shell thickness continues to increase slightly to 21 nm. Further cooling to 74 °C results in a decrease to 19.7 nm, and from 74 °C to 20 °C, the shell thickness remains nearly constant at approximately 19 nm at 20 °C. A slight decrease in the shell thickness from 21 to 19 nm during cooling in the 74–20 °C range suggests partial disassembly of the aggregates, indicating a degree of redispersion.

However, the final shell thickness at 20 °C (19 nm) remains slightly higher than the initial value (18 nm), suggesting that some aggregates persist in solution.

Considering the non-monotonic temperature behaviour of the shell thickness during heating, a more precise estimation of the LCST transition point is obtained from the cooling curve.

This transition point corresponds to the temperature at which nanoparticle aggregation ceases and the shell thickness begins to decrease, giving an approximate value of 82 °C. Notably, the LCST transition occurs over a relatively broad temperature range of 74–91 °C, highlighting the gradual and dynamic nature of the LCST phase transition of the polymer (Fig. 2).

This thermal behaviour is accompanied by significant changes in the optical extinction spectra of PEtOx-AuNPs. The formation of the polymer shell around AuNPs is evidenced by a 5.8 nm red shift in the SPR peak after ligand exchange (Fig. S5 (b), ESI†). This red shift occurs due to the increase in the dielectric constant of the AuNP environment after polymer coating. Additionally, the SPR peak exhibits noticeable broadening, indicating larger fluctuations in the dielectric constant in the PEtOx shell compared to the citrate-stabilized AuNPs.

The temperature dependence of the extinction spectra of both AuNPs and PEtOx-AuNPs was studied in detail throughout a 20–91–20 °C heating–cooling cycle. While the extinction spectrum of citrate-stabilized AuNPs remains largely unchanged across the investigated temperature range, the spectrum of PEtOx-AuNPs undergoes significant changes during both heating and cooling (Fig. S6, ESI†).

Normalization and determination of the shift were performed relative to the corresponding values at an initial temperature of 20 °C before heating.

The temperature variation significantly affects the SPR peak during both heating and cooling. This effect is particularly pronounced in the temperature range of 70–90 °C, which corresponds to the LCST transition point of the polymer (Fig. S6 (a and b), ESI†).The polymer extinction peak also exhibits changes at temperatures near the LCST transition point, but these changes are less pronounced (Fig. S6 (c and d), ESI†) compared to those observed for the SPR peak (Fig. S6 (a and b), ESI†).

The LCST transition in the PEtOx shell is clearly detected both in the temperature dependences of the spectral characteristics of the Au core SPR peak and the peak of the polymer shell (Fig. 3).

All temperature-dependent parameters—including the height of the PEtOx extinction peak, the height spectral position, and the width of the SPR peak—exhibit sharp features within the LCST transition range (76–91 °C), confirming the occurrence of this transition in the polymer shell of AuNPs. Based on the dependencies shown in Fig. 3, the LCST transition point in PEtOx-AuNPs is determined to be 82 °C. Consistent with the DLS data, light extinction measurements indicate that the LCST transition occurs over a broad temperature range of 74–91 °C. Furthermore, Fig. 3 shows that the heating–cooling cycle induces irreversible changes in the height, spectral position, and width of the extinction peaks. Therefore, this observation suggests that the aggregates formed during the LCST transition upon heating are not fully redispersed and partially persist in solution upon cooling to the initial temperature.

A detailed discussion of these temperature-dependent behaviours and the physical mechanisms is provided in the ESI†. Notably, the temperature-induced changes in the spectral characteristics of the observed SPR extinction peak in PEtOx-AuNPs are significantly more pronounced than those previously reported.[27] In summary, our results demonstrate that the LCST transition in the PEtOx-AuNP shell can be directly detected without the need for an aggregation-enhancing agent (*e.g.*,

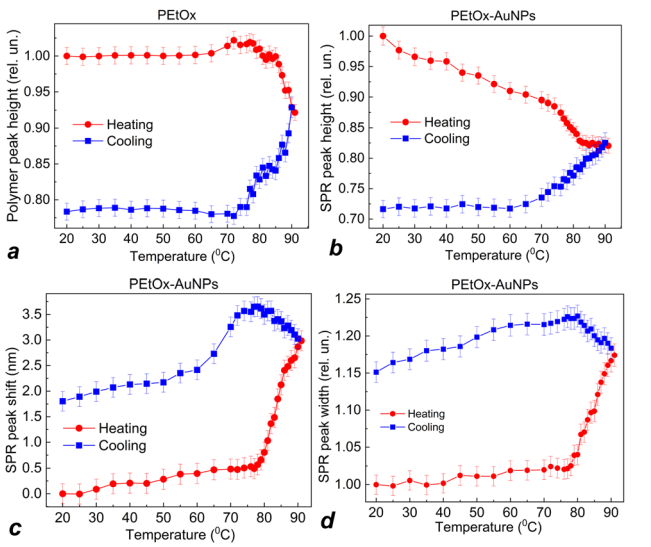

Fig. 3 Temperature dependences of extinction peak characteristics during the heating–cooling cycle in the temperature range of 20–91–20 °C: (a) PEtOx peak normalized height, (b) SPR peak normalized height, (c) SPR peak shift, and (d) normalized SPR peak width.

NaCl), thus simplifying the process of LCST transition detection.

This approach enabled us to conduct a SERS study of plasmonic photothermal nanoparticles, focusing on the changes induced by the LCST transition. The Raman spectra of PEtOx-AuNPs reveal that the vibrational spectrum of the studied samples contains frequency characteristic of xanthate-POx[34–36] in the spectral regions of 2800–3200 cm^{-1} (stretching vibrations of the C–H bond in the CH_2 and CH_3 groups) and 1200–1700 cm^{-1} (stretching vibration of the C═O bond and deformation vibrations in the CH_3 and CO–CH_2 groups), as shown in Fig. 4 and S6, ESI†. The frequencies of these vibrational modes are listed in Table 1. The intensity of the spectrum of PEtOx is relatively weak, with only high-frequency peaks in the 2800–3200 cm^{-1} region being clearly detected, while the low-frequency peaks (1200–1700 cm^{-1}) are not observed (Fig. S7, ESI†).

In contrast, the intensity of the PEtOx spectrum in the PEtOx-AuNP system increases sharply, with low-frequency peaks being reliably detected (Fig. S7, ESI†). This effect is attributed to SERS, which is a consequence of the enhancement of the Raman spectrum of the polymer in the plasmonic field of the Au core, confirming the formation of a polymer shell around the AuNPs. Notably, the intensity of low-frequency peaks increases significantly more than that of the high-frequency peaks. This phenomenon is a consequence of the fact that low-frequency peaks are closer to resonance than high-frequency peaks, which leads to their stronger plasmon enhancement.

The heating–cooling cycle, involving the LCST transition followed by aggregation in the PEtOx-AuNP system, induces two effects.

First, the intensity of the SERS spectrum of the polymer increases substantially (Fig. 4), which is due to the intensification of the plasmon enhancement occurring during the LCST transition in the polymer shell. Indeed, when the polymer shrinks during the LCST transition, the thickness of the polymer shell decreases, as a result of which the polymer chains are located closer to the Au core where the plasmon field is stronger, which leads to an increase in the enhancement of the polymer SERS. In addition, in the narrow gaps between NPs densely arranged in aggregates, plasmonic hot spots arise, in which the SERS enhancement is much higher than near the surface of isolated NPs. The formation of plasmonic hot spots near the densely arranged metal NPs in the aggregates is a well-established phenomenon in plasmonics.[37,38] Second, the Raman spectrum undergoes a significant transformation, with peak broadening in the high-frequency range, leading to a loss of the fine spectral structure.

Meanwhile, changes are also observed in the low-frequency range (Fig. 4). Specifically, the relative intensities of the peaks corresponding to C═O stretching and CO–CH_2 deformation vibrations increase significantly, with a particularly pronounced effect observed for the CO–CH_2 vibration.

In addition to peak broadening, a considerable redistribution of intensities was observed. These changes not only confirm the formation of a PEtOx shell around the AuNPs but also indicate substantial structural transformations within the PEtOx-AuNP system due to the LCST transition in the polymer shell.

The structural and optical changes observed in the Raman spectra of PEtOx-AuNPs following the LCST transition highlight the dynamic interactions between the polymer shell and the AuNP core. These results underscore the multifunctional nature of PEtOx-AuNPs, where both optical sensitivity and thermal responsiveness are crucial for practical applications. To evaluate the photothermal properties, particularly the plasmonic optical heating of these hybrid nanoparticles, we investigated their photothermal efficiency (PTE) using a continuous-wave 532 nm laser, analysing the correlation between optical absorption and heat generation.

PEtOx-AuNPs and AuNPs were analysed using Zscan-TLS[39,40] following established procedures[41] and are summarised in the ESI†. Multiple measurements at varying laser powers were conducted to minimize measurement errors.[23] Zscan-TLS is a technique used to measure the optical properties of materials by detecting changes in the refractive index caused by local heating of the sample, typically induced by a focused laser beam (Fig. S8, ESI†).

Only the light absorbed by PEtOx-AuNPs and AuNPs is converted into heat inside the surrounding medium. The photothermal efficiency (PTE) (Table 2) quantifies the fraction of light thermally absorbed relative to the total extinction (non-transmitted light) of the solution. Theoretically, this depends

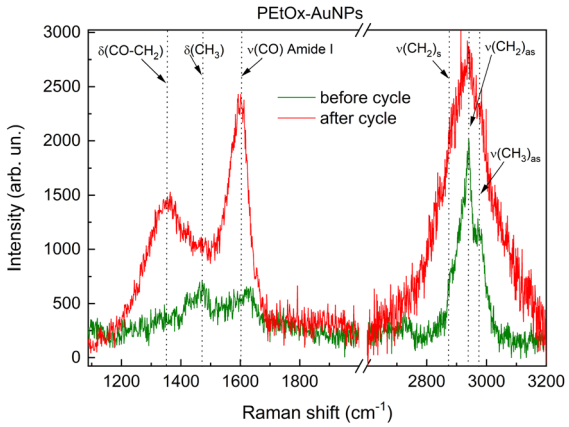

Fig. 4 Raman spectra of PEtOx-AuNPs on an Al substrate before and after heating–cooling 20–91–20 °C cycles.

Table 1 Characteristic xanthate-PEtOx vibrational modes in PEtOx-AuNPs

Vibration	Wavenumber (cm^{-1})
ν $(CH_3)_{as}$	2977
ν $(CH_2)_{as}$	2940
ν $(CH_2)_s$	2845
ν (CO)Amide I	1600
δ (CH_3)	1460
δ (CO–CH_2)	1355

Table 2 Characterization of citrate stabilized AuNPs and PEtOx-AuNPs

Sample	ζ-potential, mV[a]	λ_{max}, nm[b]	PTE%[c]
AuNPs	−35	528	83
PEtOx-AuNPs	−24	536	91

[a] ζ-potential values are represented as mean ± standard deviation (n = 3). [b] By UV-vis spectroscopy. [c] By Zscan-TLS.

on experimental factors such as nanoparticle size, shape, composition, concentration, and wavelength.[2] Quantitative insights into these properties can be obtained through theoretical approaches such as using Mie's theory, which calculates scattering, extinction, and absorption of nanoparticles of various shapes. However, theoretical procedures are often complex, and the results of these calculations are not always experimentally validated, highlighting the importance of experimental measurements. Techniques, such as light scattering spectroscopy, thermal lensing spectroscopy, and extinction spectroscopy, remain essential for characterizing AuNPs.

Hybrid PEtOx-AuNPs exhibit enhanced photothermal effects compared to AuNPs. PEtOx coating can act as a thermoresponsive shell that modifies the local refractive index and thermal conductivity around the AuNPs. Upon heating, the polymer undergoes a conformational change near its LCST, potentially facilitating more efficient heat dissipation into the surrounding medium due to a reduction in hydration and increased polymer compaction. This dynamic behavior may contribute to the observed enhancement in photothermal efficiency in Z-scan measurements. From an optical standpoint at the nanoscale, the PEtOx layer—having a refractive index intermediate between that of gold and water—can act as an impedance-matching medium, facilitating more efficient coupling of optical energy into the system. This index gradient may reduce scattering losses and enhance absorption, effectively favoring photothermal conversion over radiative loss. The LCST of the PEtOx polymer ligand plays a critical role in this enhancement, by influencing the dielectric environment around the AuNPs, which slightly tunes the SPR of the nanoparticles. As a result, the core–shell configuration of the PEtOx-AuNPs optimizes their photothermal properties, increasing their efficiency by approximately 10%, making them more effective for applications that rely on efficient heat generation.

Conclusions

In this study we successfully functionalized AuNPs through a straightforward ligand exchange method. This was confirmed by UV-vis measurements, which showed a distinct spectral shift, and ζ-potential measurements that quantitatively assessed the change in surface charge. TEM images further confirmed changes in densities around AuNPs. The temperature-responsive PEtOx coating effectively alters the local dielectric environment of the AuNPs, fine-tuning their SPR. This coating also generates a tunable SERS signal based on the LCST transition, offering exciting possibilities for dynamic sensing applications.

For the first time, we employed Zscan-TLS to evaluate the photothermal efficiencies of hybrid AuNPs, focusing on the heat generation efficiency upon photoexcitation. Notably, PEtOx-AuNPs exhibited the highest photothermal efficiency enhancement compared to AuNPs, attributed to the thermosensitive polymer layer. This layer modulates the local refractive index, shifting the plasmonic resonance and enhancing light absorption and heat generation. The functionalization of AuNPs with PEtOx shows great promise for reducing immunogenicity, making these AuNPs ideal candidates for biomedical applications such as photothermal therapy, imaging, or nanoscale heat generation.

Looking forward, functionalizing PEtOx-AuNPs with fluorescent molecules or quantum dots could enable temperature-controlled modulation of absorption, fluorescence, and Raman scattering. This opens up new opportunities for PEtOx-AuNPs as a powerful platform for the development of temperature-controlled optical switches.

Overall, this work underscores the versatility of PEtOx-AuNPs and sets the stage for their integration into next-generation optical and biomedical technologies, positioning them as a powerful platform for both scientific exploration and practical applications.

Data availability

All the data supporting the results of this study have been included within the main text and as part of the ESI†. No additional datasets were produced or examined beyond those presented.

Author contributions

O. Y. conceptualization, methodology, project administration, formal analysis, funding acquisition, visualization, investigation, writing – original draft, writing – review & editing; L. D. data curation, investigation; P. K. data curation, investigation; O. F. data curation, investigation; J. Z. data curation, investigation; G. B. methodology, data curation, investigation, writing – review & editing; T. B. methodology, data curation, investigation, writing – review & editing; C. P. data curation, investigation, formal analysis, writing; P. S. conceptualization, data curation, investigation, formal analysis, writing; and O. K. conceptualization, funding acquisition, project administration, writing – original draft supervision, writing – review & editing.

Conflicts of interest

There are no conflicts to declare.

Acknowledgements

This work received financial support from the ANR project No. ANR-22-CPJ1-0026-01, NATO SPS Programme project No. G6197, and the Ministry of Education and Science of Ukraine

projects No. 0122U001956 and 0124U001177. The University of Angers and Angers Loire Métropole are also acknowledged for a PhD grant to L. D. The authors are thankful to Prof. V. Montembault and Prof. L. Fontaine for their fruitful discussion and assistance in SEC analysis. The authors acknowledge SFR4208 SCIAM R. Mallet for the TEM images, SFR MATRIX, CARMA platform I. Freuze for mass spectrometry measurements, and B. Siegler for NMR experiments.

Notes and references

1 M. Faraday, *Philos. Trans. R. Soc. London*, 1857, **147**, 145.
2 P. K. Jain, K. S. Lee, I. H. El-Sayed and M. A. El-Sayed, *J. Phys. Chem. B*, 2006, **110**, 7238.
3 J. R. G. Navarro and M. H. V. Werts, *Analyst*, 2012, **138**, 583.
4 H. H. Nguyen, J. Park, S. Kang and M. Kim, *Sensors*, 2015, **15**, 10481.
5 O. A. Yeshchenko, S. Golovynskyi, V. Y. Kudrya, A. V. Tomchuk, I. M. Dmitruk, N. I. Berezovska, P. O. Teselko, T. Zhou, B. Xue, I. Golovynska, D. Lin and J. Qu, *ACS Omega*, 2020, **5**, 14030.
6 N. R. S. Sibuyi, K. L. Moabelo, A. O. Fadaka, S. Meyer, M. O. Onani, A. M. Madiehe and M. Meyer, *Nanoscale Res. Lett.*, 2021, **16**, 174.
7 P. N. Njoki, I.-I. S. Lim, D. Mott, H.-Y. Park, B. Khan, S. Mishra, R. Sujakumar, J. Luo and C.-J. Zhong, *J. Phys. Chem. C*, 2007, **111**, 14664.
8 R. Khandelia, A. Jaiswal, S. S. Ghosh and A. Chattopadhyay, *J. Mater. Chem. B*, 2014, **2**, 6472.
9 C. J. Mu, D. A. LaVan, R. S. Langer and B. R. Zetter, *ACS Nano*, 2010, **4**, 1511.
10 J. Shi, P. W. Kantoff, R. Wooster and O. C. Farokhzad, *Nat. Rev. Cancer*, 2017, **17**, 20.
11 M. Sarkis, G. Minassian, N. Mitri, K. Rahme, G. Fracasso, R. El Hage and E. Ghanem, *ACS Appl. Bio Mater.*, 2023, **6**, 819.
12 F. Doberenz, K. Zeng, C. Willems, K. Zhang and T. Groth, *J. Mater. Chem. B*, 2020, **8**, 607.
13 E. Cabane, X. Zhang, K. Langowska, C. G. Palivan and W. Meier, *Biointerphases*, 2012, **7**, 9.
14 A. Bordat, T. Boissenot, J. Nicolas and N. Tsapis, *Adv. Drug Delivery Rev.*, 2019, **138**, 167.
15 Y. Yuan, K. Raheja, N. B. Milbrandt, S. Beilharz, S. Tene, S. Oshabaheebwa, U. A. Gurkan, A. C. S. Samia and M. Karayilan, *RSC Appl. Polym.*, 2023, **1**, 158.
16 M. W. M. Fijten, C. Haensch, B. M. van Lankvelt, R. Hoogenboom and U. S. Schubert, *Macromol. Chem. Phys.*, 2008, **209**, 1887.
17 R. Hoogenboom, H. M. L. Thijs, M. J. H. C. Jochems, B. M. van Lankvelt, M. W. M. Fijten and U. S. Schubert, *Chem. Commun.*, 2008, 5758, DOI: **10.1039/b813140f**.
18 J.-S. Park and K. Kataoka, *Macromolecules*, 2007, **40**, 3599.
19 T. Lorson, M. M. Lübtow, E. Wegener, M. S. Haider, S. Borova, D. Nahm, R. Jordan, M. Sokolski-Papkov, A. V. Kabanov and R. Luxenhofer, *Biomaterials*, 2018, **178**, 204–280.
20 S. Zalipsky, C. B. Hansen, J. M. Oaks and T. M. Allen, *J. Pharm. Sci.*, 1996, **85**, 133.
21 T. T. H. Thi, E. H. Pilkington, D. H. Nguyen, J. S. Lee, K. D. Park and N. P. Truong, *Polymers*, 2020, **12**, 298.
22 S. Kobayashi, S. Iijima, T. Igarashi and T. Saegusa, *Macromolecules*, 1987, **20**, 1729.
23 G. Boudebs, J.-B. Zinoune, C. Cassagne and M. Chis, *Appl. Opt.*, 2023, **62**, 7669.
24 R. V. Lupusoru, D. A. Pricop, C. M. Uritu, A. Arvinte, A. Coroaba, I. Esanu, M. F. Zaltariov, M. Silion, C. Stefanescu and M. Pinteala, *Sci. Rep.*, 2020, **10**, 1.
25 Y. Wang, J. E. Q. Quinsaat, T. Ono, M. Maeki, M. Tokeshi, T. Isono, K. Tajima, T. Satoh, S.-i. Sato, Y. Miura and T. Yamamoto, *Nat. Commun.*, 2020, **11**, 1.
26 Y. Shimano, K. Sato and S. Kobayashi, *J. Polym. Sci., Part A: Polym. Chem.*, 1995, **33**, 2715.
27 V. R. de la Rosa, Z. Zhang, B. G. De Geest and R. Hoogenboom, *Adv. Funct. Mater.*, 2015, **25**, 2511.
28 O. Tzhayik, P. Sawant, S. Efrima, E. Kovalev and J. T. Klug, *Langmuir*, 2002, **18**, 3364.
29 S. A. Vorobyev, S. V. Saikova, S. A. Novikova, O. Y. Fetisova, S. M. Zharkov, A. S. Krylov, M. N. Likhatski and Y. L. Mikhlin, *ACS Omega*, 2019, **4**, 11472.
30 V. G. Deepagan, M. N. Leiske, N. L. Fletcher, D. Rudd, T. Tieu, N. Kirkwood, K. J. Thurecht, K. Kempe, N. H. Voelcker and A. Cifuentes-Rius, *Nano Lett.*, 2021, **21**, 476–484.
31 D. Pizzi, A. Nandakumar, J. P. Morrow, J. Humphries, G. Siddiqui, D. J. Creek, J. F. Quinn, J. Yin, Q. Shi, W. Cheng, K. J. Thurecht and K. Kempe, *Eur. Polym. J.*, 2024, **210**, 112964.
32 J. F. Moulder, W. F. Stickle, P. E. Sobol and K. D. Bomben, *Handbook of X-Ray Photoelectron Spectroscopy: A Reference Book of Standard Spectra for Identification and Interpretation of XPS Data*, ed. J. Chastain, 1992.
33 V. Sashuk, *ACS Nano*, 2012, **6**, 10855.
34 R. Woods and G. A. Hope, *Colloids Surf., A*, 1998, **137**, 319.
35 R. Jordan, N. West, A. Ulman, Y.-M. Chou and O. Nuyken, *Macromolecules*, 2001, **34**, 1606.
36 T. Li, H. Tang and P. Wu, *Langmuir*, 2015, **31**, 6870.
37 S. A. Maier, *Plasmonics: Fundamentals and Applications*, Springer US.
38 V. Klimov, *Nanoplasmonics*, Taylor & Francis, Andover, England, UK, 2014.
39 G. Boudebs and S. Cherukulappurath, *Opt. Commun.*, 2005, **250**, 416.
40 E. L. Falcão-Filho, C. B. de Araújo, C. A. C. Bosco, L. H. Acioli, G. Poirier, Y. Messaddeq, G. Boudebs and M. Poulain, *J. Appl. Phys.*, 2004, **96**, 2525.
41 J.-B. Zinoune, C. Cassagne, M. H. V. Werts, M. Loumaigne, M. Chis and G. Boudebs, *Chem. Phys. Lett.*, 2023, **823**, 140501.